Prediction of CCN number concentration using Measurements of Aerosol Size Distributions and Composition and Light Scattering Enhancement due to Humidity

Barbara Ervens[1,2], Michael Cubison[3,4], Elisabeth Andrews[2,3], Graham Feingold[2], John A. Ogren[2], Jose L. Jimenez[3,5], Peter DeCarlo[3,6], and Athanasios Nenes[7]

[1] Atmospheric Science Department, Colorado State University, Fort Collins, Colorado, USA

[2] NOAA Earth System Research Laboratory, Boulder, Colorado, USA

[3] CIRES, University of Colorado, Boulder, Colorado, USA

[4]School of Earth, Atmospheric and Environmental Sciences, University of Manchester, UK

[5] Dept. Chemistry and Biochemistry, University of Colorado Boulder, Colorado, USA

[6] Dept. of Atmospheric and Oceanic Sciences, University of Colorado, Boulder, Colorado, USA

[7] Dept. of Earth and Atmospheric Sciences, Georgia Institute of Technology, Atlanta, Georgia, USA

Key words: Cloud condensation nuclei, light scattering, hygroscopicity

Index terms: 0305 Aerosols and particles
0320 Cloud physics and chemistry
3311 Clouds and aerosols

- Submitted to *Journal of Geophysical Research*: 04/21/2006 -

- Revised: 9/14/2006, 2nd revision: 11/11/2006

Abstract. A cloud condensation nucleus (CCN) closure experiment is carried out using data from the Chebogue Point, Nova Scotia ground site during the International Consortium for Atmospheric Research on Transport and Transformation (ICARTT) field experiment in the summer of 2004. The number concentration of CCN at five supersaturations (~0.07% to ~0.5%) is predicted from measurements of aerosol size distribution, composition, and hygroscopic growth, and compared to measured CCN concentrations. It is shown that CCN can be predicted quite reliably using measured size distributions, a simple aerosol model to derive the mole ratio of solute to water, and the diameter growth factor *g(RH)* or the optical growth factor *f(RH)*. The mean error ranges from an overestimate in CCN of ≤ 5% at high supersaturation to a factor of 2.4 at low supersaturation with regression coefficients r^2 of 0.90 and 0.53, respectively.

The poor agreement at low supersaturation is primarily a result of high flow rates in the CCN counter that prevented small particles from growing to detectable sizes. Precise knowledge of the temperature gradient, and flow rates of the particular instrument, is essential to establish the correct supersaturation, particularly at low supersaturation, where errors translate into a large percentage of the activated number. There may also be some contribution from simplified composition assumptions, e.g. variability with size and/or mixing state. The mostly oxygenated organic, aerosol at this site could be modeled as insoluble, within the above uncertainties, from the point of view of hygroscopicity and activation. The generality of these conclusions will have to be tested at other locations.

1. Introduction

The subset of atmospheric aerosol particles known as cloud condensation nuclei (CCN) are particularly important in climate studies because they are hygroscopic and represent the particles on which cloud droplets form. Their ability to scatter and absorb radiation is influenced by ambient humidity and has important implications for radiative forcing of climate and cloud formation. The ability of an aerosol particle to act as a CCN depends on the extent to which it takes up water vapor, which in turn depends on many factors such as size and composition.

In recent years, the advent of new, commercially available instruments that measure CCN at specified supersaturation values (S) has made it more practical to extend earlier studies and examine more closely the relationship between particle size distribution, composition, hygroscopic properties, and particles' ability to act as CCN. The simultaneous measurement of all of these properties followed by their cross comparison using an activation model, often called "CCN closure", is a self-consistency check on our understanding of the system. Several studies have attempted to address the connection between aerosol growth at subsaturated conditions and their effectiveness as CCN [e.g., *Liu et al.,* 1996; *Covert et al.*, 1998; *Snider and Brenguier,* 2000; *Dusek et al.,* 2003; *Broekhuizen et al.,* 2005]. Based on these studies, parameterizations have been developed for the description of the relationship between growth factors and CCN activation [e.g., *Brechtel and Kreidenweis*, 2000]. These parameterizations require input data such as the growth factor at a given relative humidity (RH), and information on particle composition.

One of the means of determining hygroscopic growth is through measurement of the diameter growth factor *g(RH)*, defined as the ratio of the diameter of a particle at a high RH (e.g., 90%) to its dry diameter (typically 10% RH). In many studies, *g(RH)* has been determined using

Hygroscopic Tandem Differential Mobility Analyzer (HTDMA) measurements [*Rader and McMurry*, 1986]. The instrument pre-selects a size of aerosol using the first Differential Mobility Analyzer (DMA), conditions the monodisperse population at a given, higher, RH and then passes the particles through a second DMA that is also operated at the higher RH. Growth factors are thus expressed for given sizes, as selected by the first DMA, or size ranges.

In this paper we will address the utility in CCN prediction of an alternative measure of particle growth, namely the enhancement in light scattering due to uptake of water vapor. The aforementioned growth factor is typically referred to as *f(RH)* [*Covert et al.,* 1972*; McInnes et al*., 1998] and is measured in a manner analogous to *g(RH)*. The aerosol light scattering is first measured in a nephelometer at a reference (dry) RH (typically less than 40%). Upon exiting the reference nephelometer the air is exposed to a humidifier where it is conditioned to an elevated RH. The resulting "humidified light scattering" is then measured in a second nephelometer. Unlike *g(RH)*, *f(RH)* is expressed as a mean growth factor for the entire (polydisperse) population of particles. Growth factors are often quoted in terms of either two- or three-parameter fits to the data [*Kasten*, 1969; *Kotchenruther and Hobbs*, 1998], from which values at intermediate RH can be calculated. For nephelometers that measure the scattering coefficient at a number of wavelengths, e.g., 450 nm, 550 nm, and 700 nm, *f(RH)* can be reported at each wavelength. The dependence of scattering on the ratio of particle size to wavelength means that scattering at each wavelength is weighted by a different part of the size distribution [e.g., *Twomey*, 1977]. The blue wavelength (λ = 450 nm) is more sensitive to the sizes that are important for CCN closure. However, the size range of activated particles usually also includes smaller sizes that are not efficient light scatterers, even at 450 nm.

During the summer of 2004, the International Consortium for Atmospheric Research on

Transport and Transformation (ICARTT) field experiment took place in the north eastern USA and Canada. The primary goal of the experiment was to study the transport and transformation of pollution of North American origin as it moved eastwards over the Atlantic Ocean and towards Europe. An instrumented ship, and a number of instrumented aircraft and surface stations measured a variety of gas- and particulate atmospheric constituents. This study will focus on data from the ground station at Chebogue Point, Nova Scotia, where the essential components of a CCN closure experiment were available.

We use in-situ size distribution measurements together with both *f(RH)* (at three different wavelengths: λ_1 = 450 nm (blue); λ_2 = 550 nm (green); λ_3 = 700 nm (red)) and *g(RH)* measurements at a range of particle sizes in order to constrain the aerosol composition and then predict CCN number concentrations at a range of supersaturations. We explore several assumptions about the complexity of aerosol composition and provide insight into how important each of these parameters is for reliable prediction of CCN for this particular data set. We also explore a number of instrumental issues that might be considered in future studies of this kind.

2. Instrumentation

The Chebogue Point ground site (43.74 N 62.12 W) operated from July 1st to August 15th, 2004, during ICARTT and hosted a number of different teams measuring aerosol and gas phase constituents. For the purposes of our study the primary instrumentation used is listed below:

(i) CCN counter (DMT, Boulder, Colorado)

This single channel CCN counter [*Roberts and Nenes, 2005*] was programmed to step through a set of five supersaturations (S_1 - S_5) and a spectrum of the number of activated CCN (N_{CCN}) as a function of S was recorded every 30 minutes. The nominal S set points were 0.09%, 0.23%, 0.32%, 0.43% and 0.55%. However, the actual supersaturations can be slightly different for a

specific counter, due to small variations in instrument design and temperature measurement. A heat transfer and fluid dynamics model of the CCN instrument [*Nenes et al., 2001; Lance et al., 2006*] was used to predict the actual S based on recorded temperatures inside the instrument. Calibrations are used to characterize the heat transfer across the wetted walls of the instrument and then supersaturation is calculated based on the recorded temperature gradient, pressure and inlet temperature. The detailed fluid dynamical model of the instrument [*Roberts and Nenes*, 2005] is also used to calculate the (small) supersaturation variations arising from temporal fluctuations in the instrument temperature profile. Two different calculations of S are performed here and the sensitivity to these calculations will be explored. Predicted CCN are compared at the S_i calculated from the model of the instrument; in a sensitivity test we also used the nominal values of the instrument.

(ii) Differential Mobility Particle Sizer (DMPS, University of Manchester)

The DMPS [*Williams et al.*, 2000] measured the size distribution over the particle diameter range 3 nm < D_p < 810 nm, at a constant RH in the range 35 to 40%, with a temporal resolution of 10 minutes. The instrument uses two parallel DMAs coupled to Condensational Nucleus (CN) Counters (TSI Models 3025a and 3010) to classify and count particles according to their electrical mobility diameter. The nano- and long-column DMAs measured from 3 to 34 nm and 29 to 817 nm, respectively. The size distribution is measured using both DMAs simultaneously; the overlap region forms the start of the measurement cycle in both DMAs, which thus acquire particle concentration data for the 29 to 34 nm range at the same point in time.

(iii) CN Counter (TSI Model 3010): The CN counter measured the total particle concentration N. This counter has an efficiency of 50% at D_p = 10 nm and a lower detection limit of 6 nm [*Hämeri et al.*, 2002].

(iv) Humidograph system (NOAA/ESRL/GMD)

The humidograph system for measuring *f(RH)* consisted of two integrating nephelometers (TSI 3563) which measure total and back scattering at 3 wavelengths (450, 550, and 700 nm). The RH in the reference nephelometer was maintained at 30-40%, while the humidity conditioning system generated RH usually between 40-95% for measurement in the second nephelometer. (The upper limit of RH was below RH = 90% for about ~ 25% of the time.) From the combination of the 'dry' nephelometer and 'wet' nephelometer measurements an *f(RH)* value for the specific 85% / 40% values was obtained based on curve fitting. The uncertainty in the nephelometer measurements for a similar system has been calculated to be 8% [*Clarke et al.*, 2002].

The inlet to the humidograph system (and CCN counter) was equipped with an impactor to exclude particles and cloud droplets larger than 5 μm diameter, and every hour for 30 minutes a 1 μm impactor was switched in line in order to provide an indication of the difference between sub-micron and total aerosol scattering.

(v) Hygroscopicity Tandem Differential Mobility Analyzer (HTDMA, University of Manchester): g(RH) at RH = 90%

The HTDMA measured the increase in particle diameter from 35 to 90% RH for a preselected monodisperse particle population at nominal diameters of D_p = 40, 60, 89, 137, 217 and 360 nm with a temporal resolution of one hour [*Cubison et al.*, 2005]. Calibration for the offset in DMA sizing and variability in RH was achieved following the method of *Weingartner et al.* [2002] and verification of quantitative growth factor measurement using ammonium sulfate solution, referenced to well-described modeling in the literature (e.g., *Topping et al.* [2005]). In an attempt to limit kinetic effects, the HTDMA ran a residence chamber of roughly one minute between the

DMAs. The data retrieval based on an optimal estimation method was performed by the method described in *Cubison et al.* [2005]; this retrieval method was also able to determine the resolution of the instrument to be approximately 0.2 in *g(RH)* space.

(vi) Aerosol Mass Spectrometer: Composition (vacuum aerodynamic diameter D_{va} > 40 nm)

The Aerodyne Aerosol Mass Spectrometer (AMS) [*Jayne et al.*, 2000; *Jimenez et al.*, 2003] measured the size-resolved mass concentrations in the range 30 nm to 1 μm. The AMS uses an aerodynamic lens to focus the particles into a narrow beam, a roughened cartridge heater to vaporize them under high vacuum, and electron impact ionization plus a quadrupole mass spectrometer to analyze the vaporized molecules. Particle size is measured via particle time-of-flight. Below about 80 nm the transmission falls off sharply, and at ~600 nm the transmission also falls off, decreasing to around 50% at a micron particle diameter [e.g., *Jayne et al.*, 2000], which corresponds approximately to the PM_1 definition. These effects are accounted for in the data analysis process used to calculate the relative composition for the CCN model. The AMS is operated in two modes: (1) a continuous mass spectrum mode without size information; and (2) a size distribution measurement mode for selected mass-to-charge ratio settings of the quadrupole. More detailed descriptions of the AMS instrument are available in *Jayne et al*. [2000], and *Jimenez et al*. [2003], and a detailed description of the analysis technique is given by *Allan et al.* [2003, 2004]. The results of the AMS analyses for this study are presented by *Allan et al*. [2006].

(vii) Equivalent black carbon (bulk): Light absorption measurements from a Multi-Angle Absorption Photometer [MAAP; *Petzold and Schönlinner*, 2004] were converted to equivalent black carbon (EBC) concentrations using a mass absorption coefficient of 6.6 m^2 g^{-1}. This factor was empirically calculated by the Thermo Electron company, which manufactures the MAAP instrument.

3. Model calculations

The input data to the model consists of 30-min average measurements. The following input data are used:

(i) aerosol number concentration $N_{a,i}$ [cm^{-3}] in 55 size classes i (3 nm < D_p < 810 nm);

(ii) CCN concentrations at the (instrument) recorded supersaturations (S_1 - S_5);

(iii) *f(RH)* for three wavelengths, calculated at 85% RH and referenced to 40% RH;

or

(iv) *g(RH)* at six individual sizes (D_p = 40, 60, 89, 137, 217, 360 nm) at 90% RH.

The approach to predicting CCN at the prescribed supersaturations is based on model calculations of particle uptake of water vapor for measured particle size distributions. The composition of the particles is constrained using *f(RH)* (Section 3.2) and, in a second set of calculations, using *g(RH)* (Section 3.3). Additional calculations have been performed using water vapor uptake calculations based on more detailed composition information from the AMS (Section 3.5).

3.1 Hygroscopic growth

We introduce the simplified model of the equilibrium size of a wet particle of radius r, comprising soluble and insoluble fractions. The equilibrium saturation S_{eq} (= RH / 100%) is described by the Köhler equation

$$S_{eq} = \exp\left[\frac{2 M_w \sigma_s}{RT \rho_w r} - \frac{\nu\Phi M_w m_s/M_s}{\frac{4}{3}\pi \rho_{particle} r^3 - (m_s + m_{insol})}\right], \quad (1)$$

where M_w = molecular weight of water; σ_s = surface tension of the solution; R = ideal gas constant; T = temperature; ρ_w = density of water; $\nu\Phi$ ~ the van't Hoff factor, i.e., the product of the number of ions (ν) and the osmotic coefficient (Φ); M_s = molecular weight of the solute;

$\rho_{particle}$ = density of the haze particle, m_s = soluble mass ($m_{total} - m_{insol}$) , *i.e.*

$$m_s = (1 - \varepsilon) \cdot m_{total} \quad (2)$$

with m_{total} = total mass of aerosol particle and ε = insoluble mass fraction. The second term in Equation 1 (the solute term) represents the ratio of moles of solute (= f ($\nu\Phi$, M_s)) to moles of water at a given relative humidity.

Measurements of the aerosol particle composition at Chebogue Point during the measurement period show that ammonium and sulfate were the predominant inorganic components. The nitrate fraction was always small (< 5%). The mole ratio of ammonium to sulfate during five selected periods during which we did a more detailed analysis of the importance of composition (cf. Section 3.5) was always 2 or greater. Based on this analysis, we use ammonium sulfate $(NH_4)_2SO_4$ as a proxy for the soluble fraction of the aerosol. Its molecular weight is M_s = 132 g mol^{-1}, it is fully soluble, and its van't Hoff factor $\nu\Phi$ is calculated based on a parameterization of the measurements by *Kunkel* [1969]. Note that all assumptions of the physico-chemical properties also hold for periods during which the aerosol might not have been fully neutralized and ammonium bisulfate NH_4HSO_4 was the dominant inorganic solute [*Allan et al.*, 2006] because its hygroscopicity ($\propto \nu\Phi / M_s$) differs by < 5% from that of ammonium sulfate. The model approach takes into account the hygroscopicity of particles in a simplified way by modeling the mole ratio of water/solute. It does not require detailed information on different solutes that are likely to exist in the aerosol (inorganics, organics). Similar ideas haven been successfully applied by *Rissler et al.* [2004]. In Section 3.5, we refine this model to account for more complex composition, e.g. soluble organics.

3.2 Optical growth factor *f(RH)* as a composition constraint

The nephelometer measures the scattering of the aerosol population as an integrated value for the particle size range. In order to calculate the light scattering σ_{sp} of the discretized aerosol population we use Mie theory [e.g., *Bohren and Huffmann*, 1983].

$$\sigma_{sp} = \pi \sum_i r_i^2 \, Q_{scat}(m, r_i, \lambda) \, N_{a,i}, \tag{3}$$

where $N_{a,i}$ is the number concentration of particles with radius r_i (at a given RH) in size class i and the scattering efficiency Q_{scat} is a function of the particle size, refractive index m, and wavelength λ

$$Q_{scat}(m, r_i, \lambda) \propto \left(\frac{r_i}{\lambda} \right)^4. \tag{4}$$

For this application we used an average refractive index m for the total aerosol distribution of m = 1.45 + 0.005i, values derived from a comparison of the light scattering measured by a nephelometer (λ = 450 nm) for the analyzed data set to light scattering calculations (Mie theory) based on the measured aerosol size distribution measurements in this study. Calculations are performed at a reference RH = 40% ('dry') and at RH = 85% ('wet') to yield the enhancement in the total scattering σ_{sp} [m^2 m^{-3}] of the aerosol population. The optical growth factor *f(RH)* is calculated for each of the individual measured size distributions, with

$$f(RH) = \frac{\sigma_{sp}(RH = 85\%)}{\sigma_{sp}(RH = 40\%)}. \tag{5}$$

In a first approach, we apply the assumption as described in 3.1, namely that the aerosol is only composed of a soluble (with ammonium sulfate as proxy compound) fraction and an insoluble fraction ε. In order to constrain the mass fraction at each 30 min time step, the insoluble mass fraction ε is varied over the range 0% < ε < 99% (in 1% steps) until the model aerosol exhibits the same *f(RH)* as the measured data (Figure 1). This approach is similar to those that have been suggested by *Rissler et al.* [2004] and *Petters and Kreidenweis* [2006] who

suggested that hygroscopicity, and, thus, growth factors can be simply represented by the solute/water mole ratio without detailed knowledge of specific solute properties.

As described previously, a RH of 40% was used as reference for the dry state of the particles. However, it is likely that the particles contain small amounts of water at RH = 40%. In order to correct the measurements for the remaining water mass one would have to make assumptions about the composition of the particle, which is exactly the property we seek to constrain through use of *f(RH)*. The effect of this small amount of water is that predicted insoluble fractions should be slightly smaller, with commensurate effects on activated number concentration. This effect is likely to be small relative to the uncertainties in many of the other properties.

3.3 Physical growth factor *g(RH)* as a composition constraint

While *f(RH)* represents an integrated value for the size distribution, the physical growth factor g*(RH)* is derived for individual particle sizes

$$g(RH) = \frac{r(i)_{wet}(RH = 90\%)}{r(i)_{dry}} \quad . \tag{6}$$

During the experiment, growth factors were measured for six particle diameters (D_p = 40, 60, 89, 137, 217, 360 nm). The measured values as a function of particle size and time are shown in Figure 2. The fact that smaller particles exhibit higher *g(RH)* than larger ones is inconsistent with a consistent composition throughout the size range. It suggests rather that particles > 100 nm are contain less hygroscopic material.

In our first set of modeling calculations we compare the applicability of *f(RH)* and *g(RH)* as a constraint on aerosol composition. Since the particle sizes that contribute most to scattering have sizes D_p > 100 nm we average only the *g(RH)* values of the largest three sizes ($g(RH)_3$) and apply the same procedure to determine the composition (ε) as done for *f(RH)*. In additional calculations we investigate the extent to which CCN predictions change if an average of all *g(RH)* values is

applied ($g(RH)_{all}$).

3.4 Calculation of CCN number

The $(NH_4)_2SO_4/\varepsilon$ composition determined from this iterative process, using *f(RH)* and *g(RH)* as composition constraints, is then used to calculate the CCN number concentration at the five supersaturations ($S_1 - S_5$) in the CCN instrument. It can be shown (Equations 7-11) that particles which have a dry radius greater than or equal to $r_{d,c}$ (the critical dry radius) are activated at a supersaturation S_{eq} (Eq.-1) [*Pruppacher and Klett*, 1997]:

$$r_{d,c} = \left(\frac{r_{w,c}^3 (A - S_{eq}\ r_{w,c})}{A + (B - S_{eq})\ r_{w,c}} \right)^{1/3} \tag{7}$$

with

$$A = \frac{2\ M_w\ \sigma_s}{R\ T\ \rho_w} \tag{8}$$

and

$$B = \frac{\nu \Phi\ (1-\varepsilon)\ M_w\ \rho_s}{M_s\ \rho_w}$$

with ρ_s = density of the solute. The activation radius $r_{w,c}$, i.e., the wet particle size at which the particles are activated, is calculated as

$$r_{w,c} = -\frac{D}{2} + \left(\frac{D^2}{4} - E \right)^{1/2} \tag{9}$$

with

$$D = \frac{2\ B^2 A - 6\ B\ A\ S_{eq}}{3\ B\ S_{eq}^2 - 3\ B^2\ S_{eq}} \tag{10}$$

and

$$E = \frac{3\ B\ A^2}{3\ B\ S_{eq}^2 - 3\ B^2\ S_{eq}} \quad . \tag{11}$$

3.5 Refinement of aerosol composition: Organic fraction

In a second application of the model, we have refined the previous approaches by considering more complex aerosol compositions and included information on organic, inorganic and EBC mass fractions derived from AMS and MAAP measurements for five selected periods. The

inorganic fraction is assumed to be $(NH_4)_2SO_4$ and the organic fraction is assumed to have an average molecular weight M_s = 200 g mol^{-1} and van't Hoff factor $\nu\Phi$ = 1. For the model calculations, an average density for all particles has been derived using the method of comparing electrical mobility and aerodynamic diameters described by *DeCarlo et al.* [2004].

We apply this simple set of properties to the organic fraction and do not account for any deviations from ideal behavior (i.e., we assume Φ = 1) as we lack information on that from the measurements. For the same reason, we also assume that the organic fraction forms an ideal solution, i.e. we do not apply complex thermodynamic models [e.g. *Clegg et al.*, 2001; *Topping et al.,* 2004] in order to account for interactions between inorganic and organic components. Rather, we treat the water uptake on the aerosol by each component (organic/inorganic) separately, according to the ZSR approach [*Zdanovskii,* 1948; *Stokes and Robinson,* 1966]. It should be noted that the real composition of the organic fraction is likely much more complex than represented by only one compound (as defined by M, σ and $\nu\Phi$). We discuss the implications for particle growth under sub- and supersaturated conditions (i.e., growth factors and CCN activation, respectively) in Section 5.3.

4. Results

4.1 f(RH)

Figure 3 shows the measured vs. predicted CCN number concentrations based on the measured size distribution and derived composition (as represented by ε) that produced a match between measured and calculated *f(RH)* at the given wavelength. Table 1a summarizes the parameters of the regression lines for all plots in Figures 3a-c. We only compare those data for which simultaneous measurements of N_a, *f(RH)* at three wavelengths, and *g(RH)* were available (400 samples). In less than ten cases the model was unable to match the measured growth factor

294 ('No CCN calculation' in Figure 1). In these cases the growth factors exceeded the value that
295 was predicted for pure ammonium sulfate ($\varepsilon = 0$).

296 The difference between predicted and measured CCN is largest at S_1 but becomes
297 progressively smaller at $S \geq S_2$ until the best-fit regression fit approaches the 1:1 line. The
298 consistent bias at S_1 can either be explained by inappropriate assumptions in the applied model
299 that yields a CCN number that is too high or, alternatively, by uncertainties in the CCN
300 instrument, which lead to small CCN numbers: The measured small CCN number concentration
301 might suggest that the particles contain a significant fraction of insoluble material, which we
302 calculated to be $\varepsilon \sim 0.88$. However, the AMS composition data do not support such high
303 insoluble fraction as in all cases the inorganic fraction (which is composed mainly of
304 ammonium, sulfate and nitrate) was always greater than 20%. In addition, the average growth
305 factor of an aerosol population composed of ammonium sulfate and 88% insoluble material
306 would be $g(RH) \sim 1.16$, which is significantly smaller than any of the time-dependent measured
307 growth factors (Figure 2).

308 It is possible in principle that a small fraction of the organic mass sometimes goes undetected
309 by the AMS. However, the organic mass detected with the AMS compares well with the OC
310 measured with thermal-optical instruments and with the total volume or mass measured with
311 instruments such as SMPS and TEOM (Tapered Element Oscillating Microbalance). If 5-10% of
312 the organic mass was not detected by the AMS, this would likely be missed by such
313 intercomparisons due to inherent scatter, or calibration uncertainties of all instruments, but such
314 small deviations would not translate into uncertainties in the assumed inorganic/organic fractions
315 that could explain the large bias at S_1.

316 In order to explain the bias by instrumental uncertainties in the CCN counter a value of $S_1 \sim$

0.03% has to be assumed, a value deemed unrealistically low based on the instrument model calculations. Examination of the manner in which the CCN counter was operated shows that the progressive overprediction of the CCN number concentration with decreasing *S* is a result of the higher than desirable flow rates in the CCN instrument: At small *S*, the flow rate of 0.5 L min^{-1} is large enough that droplets do not reach the size threshold of 0.75 μm above which they are detected by the optical particle counter (OPC). In future applications operation at lower flow rates is recommended to allow particles to grow to detectable sizes [*Lance et al.*, 2006].

The regression coefficients for all supersaturations and *f(RH)* data increase with decreasing wavelength. This is explained by Figure 4 where we have plotted the average distribution of all 400 size distributions (dry and humidified), as well as the total scattering σ_{sp} as a function of particle size (Equation 4) for all three wavelengths, at RH = 40% and RH = 85%. It is clear that the shortest (blue) wavelength is more sensitive to small particles than the longer wavelengths. Comparing the size ranges that contribute to scattering and the critical diameters at S_1 and S_5 it becomes evident that for this size distribution, *f(RH)* contains composition information down to particle diameters of about 100 nm assuming a homogenous, internally mixed aerosol population throughout the size range. (For size distributions exhibiting a significant increase in the number of particles with decreasing size, the information content will extend to sizes smaller than 100 nm.) However, the fraction of the light scattering contributed by particles of size near the critical diameters (D_{crit1}-D_{crit5}) is very small. Thus, the good performance of the CCN closure in Figure 3, in which the activation of small particles is predicted based on scattering of larger particles, suggests relatively small differences in particle hygroscopicity over the range of sizes at this remote location where particles have had ample time to age. This closure exercise would likely be less successful e.g. in an urban area where the sources and composition of the particles around

340 D_{crit}, and the particles that dominate light scattering exhibit greater variability.

341 In Figure 5, we show the corresponding insoluble fractions ε that are required in order to
342 match the measured *f(RH)*. Using the three *f(RH)* values, the predicted average is $\varepsilon \sim 0.63$. An
343 error in the nephelometer measurements and, thus, in *f(RH)* of about 8% translates into an error
344 $\Delta\varepsilon \sim 0.15$ at $\varepsilon \sim 0.63$. Approximately the same composition is predicted at all three wavelengths.
345 The successful prediction of CCN based on this composition which includes particle diameters <
346 100 nm (e.g., at S_5) suggests that the assumption of an internal mixture composition that is
347 invariant with size is appropriate and any differences in hygroscopicity throughout the size range
348 are small. Thus, for these conditions we show that composition information from any range of
349 the size distribution can be used as a proxy for the whole size range. In the case of varying
350 composition throughout the particle sizes, the application of *f(RH)* in order to determine the
351 composition for CCN relevant sizes is likely to be less successful.

352 ***4.2 g(RH)***

353 The growth factors *g(RH)* were determined for six different sizes (40-360 nm). For some
354 periods there is no clear difference between the measured growth factors in this size range
355 (Figure 2); however, in general, the largest particles exhibit smaller *g(RH)* values than particles <
356 100 nm. This behavior cannot be explained by an internally mixed aerosol population as, all else
357 being equal, smaller particles should have smaller *g(RH)* due to the Kelvin (curvature) effect
358 (first term on the right hand side of Eq.-1). In a first approach we compare the data derived based
359 on both approaches of growth factor measurements (*f(RH)* and *g(RH)*) and we use $g(RH)_3$ (i.e.
360 D_p > 100 nm) since scattering is also dominated by particle sizes above this threshold. In
361 addition, we also summarize regression parameters in Table 1a and Figure 6 that were derived
362 based on an average of all size growth factors $g(RH)_{all}$.

363 The results in Figure 6 have been obtained using the same procedure as described in section 4.1
364 and Figure 1, except that now the water vapor uptake characteristics of the aerosol model are
365 constrained by *g(RH)*. The composition (i.e., ε) is varied until the model matches the measured
366 value $g(RH)_3$. This calculation is consistent with that of *Rissler et al.* [2004]. We see that the
367 model using $g(RH)_3$ leads to an overestimate of the CCN number concentration that is small at
368 high *S* but increases with decreasing *S*, and has less scatter than the comparison based on *f(RH)*
369 (Figure 3). The high bias in predicted CCN at S_1 is again primarily attributed to the large flow
370 rate in the CCN counter and the inability of the OPC to detect the growing droplets.
371 (Explanations based on composition variability with size, and/or mixing state cannot be ruled out
372 but are deemed less likely.) At S_1, there is some small improvement in the slope of the regression
373 (Table 1a) when an attempt is made to account for variability of composition with size (compare
374 $g(RH)_3$ and $g(RH)_{all}$), but there remains a very strong overestimate in predicted CCN
375 concentration. For this simple aerosol model, the composition measurements do not support the
376 very high insoluble fraction ($\varepsilon = 0.88$) that would be required to match the small CCN number at
377 low *S*. The general bias towards larger values of predicted CCN has been observed in previous
378 closure studies for similar conditions, e.g. by *Broekhuizen et al.* [2005] who attributed the bias to
379 poor size resolution.

380 In Figure 5, the predicted insoluble fractions ε based on *g(RH)* are compared to those obtained
381 using *f(RH)*. It is evident that there is a systematic difference, with smaller insoluble fractions
382 derived from $g(RH)_3$ (average ± standard deviation $\varepsilon \sim 0.53 \pm 0.14$, compared to $\varepsilon = 0.63 \pm 0.16$
383 based on *f(RH)*). If the growth factors of the more hygroscopic particles are also included
384 ($g(RH)_{all}$), $\varepsilon = 0.39 \pm 0.16$ is predicted.
385

4.3 Comparison of *f(RH)* and *g(RH)* results

4.3.1 Agreement in predicted CCN

Both Figures 3 and 6 (and Table 1) show a correlation $r^2 > 0.8$ between the predicted and measured CCN number concentrations for both *f(RH)* and *g(RH)* at $S \geq S_3$, with results improving with increasing *S*. In order to check if this is based on common agreement for the same data points, Figure 7 compares the calculated CCN numbers based on $f(RH)_{green}$ and $g(RH)_3$. The agreement is worst at S_1 since use of $g(RH)_3$ leads to a greater overestimate of the CCN number than the data based on $f(RH)_{\text{green}}$ (see slope of regression lines in Table 1a). In Figure 5 we showed that the insoluble fraction ε derived from modeling *f(RH)* was about 0.63 whereas the corresponding value based on $g(RH)_3$ is lower ($\varepsilon \sim 0.53$). However, at the higher supersaturations S_2 - S_5 predictions based on *g(RH)* and $f(RH)_{green}$ lead to CCN numbers that exhibit a small difference between the two predicted CCN number concentrations, which is reflected by the slope of the regression line of 1.15 to 0.98 at low and high *S*, respectively (Table 1b, Figure 7). At S_2-S_4 , there are apparently two separate groups of data: Most of the points are close to the 1:1 line while a small fraction of the points shows a distinctly greater slope. The measurements for these few points were contiguous in time during a period with high organic fraction (cf. Section 4.4.1, period 1). However, even a closer analysis of all available measurements for period 1 does not lead to any comprehensive explanation for the differences between the CCN calculated from *g(RH)* and *f(RH)* compared to the other data points.

4.3.2 Assumption of constant ε

In order to explore the extent to which the knowledge of the effective insoluble fraction is important for CCN prediction, we assumed a constant ε (37% $(NH_4)_2SO_4$/ 63% insoluble) for all data based on the *f(RH)* composition modeling. Note that this ε could not have been known *a*

409 *priori.* The results using $\varepsilon = 0.63$ are shown in Figure 8. In addition, we compare the parameters
410 of the regression lines for these plots in Table 1a for the same data points as compared in Figures
411 3 and 6. At all supersaturations the slopes of the regression lines are comparable to those derived
412 using variable ε. The variation of ε in the range we predict based on *f(RH)* and *g(RH)*
413 measurements leads to the same predicted CCN number concentration at higher *S*. This suggests
414 that small differences in hygroscopicity (as implied by changing ε in Eqs.1-3, as a possible proxy
415 for other aerosol composition properties in Eq.-1) from the average for the period play a rather
416 weak role for the activation of the aerosol sampled at Chebogue Point.

417 **4.4 Increasing the complexity of aerosol composition**

418 **4.4.1 Inorganic, organic, insoluble and equivalent black carbon fraction**

419 Table 2 contains information about five different selected periods that have been chosen in
420 order to analyze more closely the effects of aerosol composition on the calculated CCN. The
421 periods have been selected based on differences in composition, mass loading, and aerosol
422 history. However, they can be classified into two broad groups: Periods 1, 2, and 5 exhibit high
423 organic fractions, while during periods 3 and 4 the inorganic fraction dominates. For each of
424 these periods we have defined mass fractions for inorganics, organics and EBC based on the
425 AMS and MAAP measurements. Particle composition is assumed to be constant with size and all
426 particles are assumed to contain an internal mixture of the species present in the same mass
427 proportions as in the average composition. Clearly this is still a simplified model since *g(RH)*
428 measurements indicate a change in composition with size (Figure 2).

429 We assumed the properties for $(NH_4)_2SO_4$ for the inorganic fraction, since ammonium and
430 sulfate are the predominant inorganic solutes (and NH_4HSO_4 has very similar hygroscopic
431 properties), even though the aerosols had a more complex inorganic composition. Most of the

organics at Chebogue Point can be classified as oxygenated organic aerosols (OOA) [*Allan et al.*, 2006]. Recent results of field experiments in Tokyo indicate that about 90% of OOA detected with an AMS are water-soluble, as measured with the PILS-OC (Particle-in-liquid-sampler, organic carbon) technique [*Kondo et al.*, 2006].

In order to check our previous predictions of the effective insoluble fraction ε we show in Figure 9 the measured organic fractions and equivalent black carbon fractions and the insoluble fraction as predicted from the calculations described in Section 4.1, based on $f(RH)_{green}$ as a constraint (the error bars represent the standard deviation based on all predicted ε in the respective period). Assuming that all organics are effectively insoluble and the insoluble fraction of the aerosol is composed only of EBC and organics, the difference between the measured and the predicted insoluble fractions is in all cases less than 10%. The inference that almost all of the organic mass can be modeled as effectively insoluble seemingly contradicts the previous classification of OOA as water-soluble. A possible reason for this discrepancy might be differences between the OOA solubility in Tokyo and Chebogue Point. A more likely explanation is that particles at RH = 85 % do not contain much water (water/solute mass ratio ~ 1) and, thus, organics of limited solubility might not be fully dissolved. At high ionic concentrations in the aqueous phase organics might form a separate phase due to the 'salting out' effect which leads to an even smaller apparent solubility. In the PILS-OC instrument the organic mass is diluted to typical concentrations of $1\text{-}2\cdot10^{-4}$ g L^{-1} water (100-200 ppb kg^{-1} [R. Weber, personal communication]). Our results suggest that most of the water-soluble organic carbon determined in analyses such as the PILS-OC might not influence the particle growth by water uptake at subsaturated conditions.

In Figure 10 the comparison is shown of the predicted CCN number concentration based on

455 $f(RH)_{green}$ using the $(NH_4)_2SO_4/\varepsilon$ model and the more complex directly-measured composition
456 described in Table 2. Both are plotted as a function of the measured CCN concentrations. Unlike
457 the composition variation performed in Section 4.1 and 4.2 where ε was varied over the total
458 aerosol mass, the variation of the insoluble fraction is now only done over the organic fraction
459 (ε'). In most cases, this approach is not able to match the measured $f(RH)_{green}$ values since it
460 requires even more insoluble mass than is represented by ε' =1 (organic + EBC fraction =
461 insoluble). Therefore we show the predicted CCN for the boundary value of $\varepsilon' = 1$ (i.e., organics
462 modeled as completely insoluble) for all periods. It is noted that in some cases when the AMS
463 and MAAP data are included in the calculations, there is a marginal improvement in the
464 predicted number of CCN (e.g., period 5). However, in general the benefit of the additional
465 complexity in the aerosol model is small.

466 In previous CCN closure studies it has been assumed that all organics are insoluble, and that
467 the remainder of the aerosol mass contains additional insoluble material. Even this assumption
468 can lead to an overestimate of the CCN numbers by about 25% [*Broekhuizen et al.,* 2005]. In this
469 latter study, it is suggested that the agreement in the CCN closure might be improved with more
470 detailed information on (i) size-resolved composition and (ii) the mixing state of the aerosol
471 population, i.e. the existence of completely insoluble and soluble particles of the same size
472 (external mixture).

473 For our model calculations we have assumed an internal mixture for all particles. As *g(RH)*
474 measurements are performed for single particles at selected sizes an externally mixed aerosol
475 population will result in a growth factor distribution. Based on the uncertainty of the instrument
476 ($\Delta g(RH) = 0.2$) we cannot fully exclude the possibility of externally mixed aerosols. However,
477 the hygroscopicity of particles having different compositions was very similar, i.e. within the

range of the instrument's uncertainty. The uncertainty in *g(RH)* of about 0.2 translates into $\Delta\varepsilon \sim 0.3$. As shown in Section 4.3.2, the assumption of a constant value for ε did not change the predicted CCN significantly for the retrieved range of ε between ~ 0.3 and 0.9 (Figure 5). Nevertheless, inaccuracies in *g(RH)* measurements might have a significant bearing on ε and need to be considered in retrievals of this kind.

4.4.2 Additional information on composition

Size-resolved composition: In addition to the size-averaged composition given in Table 2, we have used size-resolved information on composition. Information was available for particles greater than D_{va} = 100 nm (vacuum aerodynamic diameter, *DeCarlo et al.* [2004]) for three different size ranges (100-250 nm, 250-700 nm, >700 nm). The EBC fraction is assumed constant for all size classes since it was determined from the absorption properties of the total aerosol population and we have no means of apportioning it by size. The insoluble fraction of these calculations was assumed to be $\varepsilon' = 1$, as in Section 4.4.1. Due to the lack of further information we had to make assumptions about the composition of particles smaller than D_{va} = 100 nm and varied their composition between 99% insoluble and completely soluble ammonium sulfate. Even this refinement of the composition did not lead to any improvement in the agreement between measured and predicted CCN numbers compared to Figure 10. Results are therefore not shown.

Refractive index of organic fraction: The refractive index of the internally mixed inorganic/organic aerosol, as used in the model calculations in the previous sections, is based on the consistency between measured optical properties and calculations based on aerosol size distributions over the entire measurement campaign. The refractive index of organic aerosol constituents is poorly constrained. Since no further specification of the organic fraction for our

specific data set is available, we have explored the possible effects of refractive index of the organics by considering the range of values found in literature studies for organics in different locations. We have found that even the variation from $m = 1.53$ [*Malm et al.*, 2005], to $m = 1.43 - 0.0035$ i [*Gelencser et al.*, 2004] does not lead to any significant change in predicted CCN number concentration. (In the interests of brevity, results are not shown.)

Density of organic fraction: The densities given in Table 2 represent average densities for the total aerosol population during the individual periods, derived from the closure of the AMS and SMPS size distributions [*DeCarlo et al.*, 2004]. The average density of OOA which were predominant at Chebogue Point has been determined as $\rho_{org} = 1.4$ g cm^{-3} [*Cross et al.*, 2006]. If we disregard the average densities used in the previous section, but use the explicit densities for all mass fractions as individual input parameters we did not observe any significant improvement in the prediction of CCN.

5. Discussion

5.1 Critical radius, *S* and size distribution

Figures 3, 6 and 7 show higher correlation coefficients r^2 (Table 1) between measured and predicted CCN number at higher supersaturation for both *f(RH)*- and *g(RH)*-derived values. In this section we discuss the reasons for higher uncertainty in CCN prediction at low *S*. The relationship between the properties of an activated particle and the critical supersaturation is given by Equations 7 through 10. By assuming a uniform composition throughout the size distribution we can determine the minimum dry size ($r_{d,c}$ in Equation 8) of the activated particles for any given size distribution and supersaturation. In Figure 11, we show the average of all 400 size distributions, the cumulative number concentration and the two average critical diameters (D_{crit1} and D_{crit5}) at S_1 and S_5, respectively. We assume an uncertainty in the activated sizes of

one size bin (dashed, vertical lines). Since the diameter bins in the size distribution are logarithmically distributed, this assumption leads to the same relative uncertainty in size. This uncertainty translates into a difference in activated particle numbers ΔN_S as shown by the differences between the horizontal lines at each of the critical diameters. We calculate the relative error δ

$$\delta = \frac{\Delta N_S}{N_S^{tot}} \tag{12}$$

in the total number of activated particles N_S^{tot} and find that δ_1 = 194/412 = 0.47; and δ_5 =152/1127 = 0.13). At low S (i.e. large sizes), δ is about 3.5 times greater than at high S. This is because in the latter case a major fraction of the aerosol population is activated, and any uncertainties in activation of additional particles represent a smaller fraction of the total activated number that leads to a smaller relative change. (The magnitude of these differences will vary with size distribution shape but the general picture is clear.) This estimate of uncertainty only explains the scattering of the points around the regression line (precision). Any systematic bias as explained previously, e.g. due to instrumental uncertainties, leads to error in the accuracy of the CCN predictions (intercept and slopes of regression lines) that are independent of the relative uncertainty (Table 1).

5.2 Calculation of supersaturation

As stated in Section 2, the nominal values of S_1 have been corrected by means of the model by *Lance et al.* [2006] in order to account for small temporal deviations in the temperature profile in the CCN counter. In order to explore to what extent this correction of S at each 30 min time step improves agreement between predicted and measured CCN, we repeated the calculations from Figure 3b ($f(RH)_{green}$) but used the nominal S values (S_1 = 0.09%, S_2 = 0.21 %, S_3 = 0.32%, S_4 = 0.43% S_5 = 0.55%) as specified by the instrument for the duration of the experiment. The results

547 are shown in Figure 12 and the corresponding regression parameters listed in Table 1a. For $S \geq$
548 S_2, the assumption of the constant nominal supersaturation values over the whole time period
549 does not bias the results significantly, for the reasons discussed in Section 5.1.

550 **5.3 Complexity of organic fraction**

551 As pointed out previously, no information on the organic properties relevant for hygroscopicity
552 could be derived based on the AMS data. This omission leads to some uncertainties in the
553 description of aerosol composition and hygroscopicity. The set of properties we have chosen for
554 the organic fraction reflects a single compound with a relatively small molecular weight (M_s =
555 200 g mol^{-1}), that does not affect surface tension, and that forms an ideal mixture with other
556 (inorganic) water-soluble compounds. This representation of the organic fraction is greatly
557 simplified as it has been shown that the organic fraction of atmospheric aerosol can be composed
558 of hundreds of different compounds with a broad range of physico-chemical properties. A large
559 fraction of this organic fraction can be composed of high molecular weight components that
560 reduce the surface tension of aqueous particles and might not be fully miscible with water [e.g.,
561 *Decesari et al.*, 2000].

562 As shown in the modeling study by *Ervens et al.* [2005], at sub-saturated conditions, the
563 particle growth is dominated by the solute term ($\propto r^{-3}$; second term in Eq.-1) as the Kelvin term
564 ($\propto r^{-1}$; first term in Eq.-1) is small at small particle radii. Thus, hygroscopic growth is mainly
565 determined by molecular weight M_s and the van't Hoff factor $\nu\Phi$. If the van't Hoff factor also
566 increases with increasing molecular weight (e.g. the polarity and water-miscibility of the
567 compound decrease) both parameters will have an opposite effect. In general, organic
568 compounds can reduce the surface tension of aqueous particles which in turn decreases the
569 critical diameter of activation (Eqs. 7-11). High molecular weight compounds have the most

distinct effect on surface tension reduction. However, the surface tension of aqueous solutions is concentration dependent, and with increasing particle size the solutions are more dilute and the surface tension effect is reduced. We cannot quantify the extent of which organic properties counter each other. However, we point out that these properties should be considered together, and that their combined effects might weaken the influence of organic properties on hygroscopic growth and particle activation.

6. Summary and conclusions

6.1 What is the relative usefulness of *f(RH)* vs. *g(RH)*?

We have used measured size distributions and optical (*f(RH))* or physical (*g(RH))* hygroscopic growth factor measurements at RH = 85% and RH= 90%, respectively, to predict CCN number concentrations. The data were obtained over a period of four weeks during July/August 2004, at Chebogue Point, Nova Scotia, Canada, as part of the ICARTT study.

To our knowledge this is the first study in which

(i) *f(RH)* has been used to extrapolate growth information of aerosols at subsaturated conditions to their CCN activity and

(ii) the resulting CCN number predictions have been compared to those based on *g(RH)* measurements.

The current results suggest that for this data set either of these growth factors can be used to give reliable predictions of CCN number at supersaturations $S > \sim 0.3\%$. We hypothesise, based on the current analysis, that similar success could have been achieved at lower *S*, had lower CCN flow rates been applied during the experiment, but this cannot be verified *a posteriori*. In addition, we cannot completely rule out the possibility that assumptions about composition at the large particle sizes and/or uncertainty in *g(RH)* measurements play a role in the poor retrievals at

low *S*.

It should also be pointed out here that *f(RH)* retrievals may be less effective if the composition of the aerosol population vs. size is not as homogeneous as in the present study. In the presence of several modes that are composed of different species, as more typically observed in an urban area, it is unclear how useful the observed growth characteristics based on *f(RH)* will be for inferring CCN properties.

6.2 What information is most crucial for CCN prediction?

The data set acquired at Chebogue Point during the ICARTT field study included detailed information on aerosol properties, namely time-resolved measurements of size distribution, number concentration, and size-resolved composition. In addition, three different *f(RH)*, *g(RH)* at six different particle sizes, and a sophisticated approach to determine the exact supersaturation at which the CCN number concentration was measured, were available. Such a detailed data set is rarely available from field studies. Based on our numerous sensitivity tests, we provide guidance in Table 3 as to what information is most crucial for future successful CCN closure experiments for similar conditions. We caution that these conclusions pertain specifically to the data from Chebogue Point and may not always be appropriate. As shown in Table 3, the most important information for CCN closure is the measured aerosol size distribution and the supersaturation. A simple representation of aerosol composition based on an internally mixed soluble/insoluble mixture, constrained by either *g(RH)* or *f(RH)*, appears to be quite adequate, especially at high supersaturations. This supports the notion that the water uptake by oxygenated organic aerosol in concentrated solutions is negligible and the organic fraction can be modeled as water-insoluble (Eqs.-1 and 2). Temporal variation in composition, and even the variability in composition with size (e.g., as reflected in *g(RH)* measurements), does not appear to be of great importance during

616 the period of study at Chebogue Point even in periods when organic species clearly dominate the
617 aerosol mass. Attempting to refine the composition using measured equivalent black carbon and
618 organic fractions does not contribute significantly to an improvement in the agreement between
619 predicted and measured CCN number concentrations. If hygroscopic growth information is
620 unavailable, predictions of CCN may still be feasible provided some *a priori* composition
621 information is available (e.g. insoluble fraction and appropriate parameterization of the solute
622 properties). This conclusion is in general agreement with the parameterization by *Fitzgerald*
623 [1975] that shows a correlation between the insoluble fraction and CCN number for a constant
624 composition of an aerosol population that is internally mixed.

625 Note that the requirement of accurate knowledge of S in the CCN instrument is important for
626 successful closure, but not for independent CCN predictions. Measured size distribution and
627 hygroscopic information should suffice for routine CCN predictions. Similar conclusions have
628 been drawn by *Rissler et al.* [2004] and *Dusek et al.* [2006] based on analysis of Brazilian
629 biomass burning aerosol and aerosol in central Germany, respectively. However, in these latter
630 studies the lowest supersaturation at which CCN analyses were performed were 0.33% and 0.4%,
631 respectively, which corresponds approximately to S_3 and S_4 in our study. In all these studies, it
632 has been consistently found that with decreasing supersaturation the CCN measurements are
633 more sensitive to instrumental conditions and counting statistics.

634 CCN closure studies describe particle activation under equilibrium conditions. They represent
635 an important step towards our understanding of the role of aerosol particles in cloud formation
636 processes. In order to give a more realistic picture of cloud formation, dynamic processes also
637 have to be considered as has been done in a recent study by *Ervens et al.* [2005], who examined
638 the effect of composition on cloud droplet number concentration. There it was shown that only

639 significant changes (~ factor of 5) in the solute term will change the cloud drop number
640 concentration appreciably (~ 15%), with the importance increasing with decreasing updraft
641 velocities and increasing aerosol number concentration. Sensitivity to composition in CCN
642 measurements does not necessarily translate into sensitivity in drop number concentration as in a
643 rising air parcel both the time for particle growth and the amount of available water vapor are
644 limited and, thus, effects of competition for water vapor might influence the growth rates of
645 particles.

646 Further aerosol measurements and model studies are required to extend our understanding of
647 the relationship between aerosol and cloud properties. It remains to be seen to what extent the
648 conclusions we have drawn from our current study hold true for other locations and aerosol
649 conditions where there is more complexity in aerosol composition and mixing state and to which
650 aerosol activation behavior can be parameterized in order to describe cloud processes properly.

651

652 **Acknowledgements.** We thank James Allan (University of Manchester), J. Alex Huffman
653 (University of Colorado), Doug Worsnop, Eben Cross, Megan Northway, and Manjula
654 Canagaratna (Aerodyne Research Institute) for AMS operation and data processing and Patrick
655 Sheridan and Anne Jefferson for building, setting up and operating the NOAA/ESRL
656 instrumentation in the field. The DMPS and HTDMA instruments were deployed by the
657 University of Manchester and M. Cubison was supported through NERC studentship no 06424
658 as a University of Manchester student during the period of the field campaign and initial
659 analysis. BE, EA, GF, and JO acknowledge funding from the NOAA Climate Goal. JLJ, MC,
660 and PFD thank NSF (CAREER grant ATM-0449815) and NOAA (grant NA05OAR4310025)
661 for funding. PFD is grateful for an EPA STAR Fellowship (FP-91650801).

662 **References**

663 Allan, J. D., J. L. Jimenez, P. I. Williams, M. R. Alfarra, K. N. Bower, J. T. Jayne, H. Coe, and
664 D. R. Worsnop (2003), Quantitative sampling using an Aerodyne aerosol mass spectrometer 1.
665 Techniques of data interpretation and error analysis, *J. Geophys. Res.*, *108*(D3), 4090,
666 doi:10.1029/2002JD002358.

667 Allan, J. D., H. Coe, K. N. Bower, M. R. Alfarra, A. E. Delia, J. L. Jimenez, A. M. Middlebrook,
668 F. Drewnick, T. B. Onasch, M. R. Canagaratna, J. T. Jayne, and D. R. Worsnop (2004),
669 Technical note: Extraction of chemically resolved mass spectra from Aerodyne aerosol mass
670 spectrometer data. *J. Aerosol Sci.*, *35*, 909–922.

671 Allan, J. D., H. Coe, J. L. Jimenez, J. A. Huffman, P. DeCarlo, M. J. Cubison, D. Worsnop, M.
672 Northway, M. Canagaratna, E. S. Cross, G. Coulson, Q. Zhang, A. Goldstein, B. Williams, D.
673 Millet, J. Ogren, E. Andrews, P. Sheridan, A. Jefferson, N. M. Kreisberg, S. V. Hering, L.
674 Russell, S. Gilardoni, P. Quinn (2006), In situ measurements of particle composition at
675 Chebogue Point during ICARTT, *J. Geophys. Res.*, submitted.

676 Bohren, C. F., and D. R. Huffmann (1983), *Absorption and scattering by small particles*, Wiley,
677 New York.

678 Brechtel, F. J., and S. M. Kreidenweis (2000), Predicting particle critical supersaturation from
679 hygroscopic growth measurements in the humidified TDMA. Part I: Theory and sensitivity
680 studies, *J. Atmos. Sci., 57*, 1854-1871.

681 Broekhuizen, K., R. Y.-W. Chang, W. R. Leaitch, S.-M. Li, J. P. D. Abbatt (2005), Closure
682 between measured and modeled cloud condensation nuclei (CCN) using size-resolved aerosol
683 compositions in downtown Toronto, *Atmos. Chem. Phys. Discuss*., *5*, 6263-6293.

684 Clarke, A. D., S. Howell, P. K. Quinn, T. S.Bates, J. A. Ogren, E. Andrews, A. Jefferson, A.

685 Massling, O. Mayol-Bracero, H. Maring, D. Savoie, and G. Cass (2002), INDOEX aerosol: A
686 comparison and summary of chemical, microphysical, an optical properties observed from
687 land, ship and aircraft, *J. Geophys. Res., 107*, D19, 8033, doi: 10.1029/2001JD000572.
688 Clegg, S. L., J. H. Seinfeld, and P. Brimblecombe (2001), Thermodynamic modelling of aqueous
689 aerosols containing electrolytes and dissolved organic compounds, *J. Aerosol Sci.*, 32(6), 713-
690 738.
691 Covert, D. S., R. J. Charlson, and N. C. Ahlquist (1972), A study of the relationship of chemical
692 composition and humidity to light scattering by aerosols, *J. Appl. Meteor., 11***,** 968–976.
693 Covert, D. S., J. L. Gras, A. Wiedensohler, F. Stratmann, Comparison of directly measured CCN
694 with CCN modeled from the number-size distribution in the marine boundary layer during
695 ACE 1 at Cape Grim, Tasmania (1998), *J. Geophys. Res., 103(D13)*, 16597-16608,
696 10.1029/98JD01093.
697 Cross, E. S., P. Davidovits, T. B. Onasch, J. T. Jayne, D. K. Lewis, M. Canagaratna, and D. R.
698 Worsnop (2006), Aerosol particle density determination using light scattering in conjunction
699 with mass spectrometry, *Aerosol Sci. Technol.*, in preparation.
700 Cubison, M., Coe, H., and Gysel, M. (2005), A modified hygroscopic tandem DMA and a data
701 retrieval method based on optimal estimation, *J. Aerosol Sci.* 36(7), 846-865.
702 DeCarlo, P., J. G. Slowik, D. Worsnop, P. Davidovits, and J. Jimenez (2004), Particle
703 morphology and density characterization by combined mobility and aerodynamic diameter
704 measurements. Part 1: Theory, *Aerosol Sci. Technol*., *38*, 1185–1205, doi: 10.1080/
705 027868290903907.
706 Decesari, S., M. C. Facchini, S. Fuzzi, and E. Tagliavani (2000), Characterization of water-
707 soluble organic compounds in atmospheric aerosol: A new approach, *J. Geophys. Res* 105, D1,

1481-1489.

Dusek, U., D. S. Covert, A. Wiedensohler, C. Neusüß, D. Weise, and W. Cantrell (2003), Cloud condensation nuclei spectra derived from size distributions and hygroscopic properties of the aerosol in coastal south-west Portugal during ACE-2, *Tellus, 55B*, 35-53.

Dusek, U., G. P. Frank, L. Hildebrandt, J. Curtius, S. Walter, D. Chand, F. Drewnick, S. Hings, D. Jung, S. Borrmann, and M. O. Andreae (2006), Size matters more than chemistry in controlling which aerosol particles can nucleate cloud droplets, *Science*, *312*, 1375-1378.

Ervens, B., G. Feingold, and S. M. Kreidenweis, The influence of water soluble organic carbon on cloud drop number concentration (2005), *J. Geophys. Res.*, *110*, D18, D18211, doi: 10.1029/2004JD005634.

Fitzgerald, J. W., Approximation formulas for the equilibrium size of an aerosol particle as a function of its dry size and composition and the ambient relative humidity (1975), *J. Appl. Meteor. 14*, 1044-1049.

Gelencsér, A. (2004), *Carbonaceous Aerosol*, Springer, Dordrecht.

Hämeri, K., C. D. O'Dowd, and C. Hoell (2002), Evaluating measurements of new particle concentrations, source rates, and spatial scales during coastal nucleation events using condensation particle counters, *J. Geophys. Res.*, *107*(D19), 8101, doi:10.1029/ 2001JD000411.

Jayne, J. T., D. C. Leard, X. Zhang, P. Davidovits, K. A. Smith, C. E. Kolb, D. R. Worsnop (2000), Development of an aerosol mass spectrometer for size and composition analysis of submicron particles, *Aerosol Sci. Technol.*, *33*, 49-70.

Jimenez, J. L., J. T. Jayne, Q. Shi, C. E. Kolb, D. R. Worsnop, I. Yourshaw, J. H. Seinfeld, R. C. Flagan, X. Zhang, K. A. Smith, J. Morris, and P. Davidovits (2003), Ambient aerosol sampling

731 with an aerosol mass spectrometer, *J. Geophys. Res., 108*(D7), 8425, doi:10.1029/
732 2001JD001213.
733 Kasten, F. (1969), Visibility forecast in the phase of pre-condensation, *Tellus*, *21*, 631-635.
734 Kondo, Y., Y. Miyazaki, N. Takegawa, T. Miyakawa, R. J. Weber, J. L. Jimenez, Q. Zhang, and
735 D. R. Worsnop (2006), Oxygenated and water-soluble organic aerosols in Tokyo. *J. Geophys.*
736 *Res.*, submitted.
737 Kotchenruther, R. A., P. V. Hobbs, and D. A. Hegg (1999), Humidification factors for
738 atmospheric aerosols off the mid-Atlantic coast of the United States, *J. Geophys. Res., 104*,
739 2239-2251.
740 Kunkel, B. A. (1969), Comments on "A generalized equation for the solution effect in droplet
741 growth", *J. Atmos. Sci., 26*, 1344-1346.
742 Lance, S., J. Medina, J. N. Smith, and A. Nenes (2006), Mapping the operation of the DMT
743 continuous flow CCN counter, *Aerosol Sci. Technol., 40*, 4, 242-254.
744 Liu, P. S. K., W. R. Leatich, C. M. Banic, , S.-M. Li, , D. Ngo, and W. J. Megaw (1996), Aerosol
745 observations at Chebogue point during the 1993 North Atlantic Regional Experiment:
746 Relationships among cloud condensation nuclei, size distribution, and chemistry, *J. Geophys.*
747 *Res. 101*, D22, 28971-28990.
748 Malm, W. C., D. E. Day, C. Carrico, S. M. Kreidenweis, J. L. Collett, Jr., G. McMeeking, T.
749 Lee, J. Carrillo, and B. Schichtel (2005), Intercomparison and closure calculations using
750 measurements of aerosol species and optical properties during the Yosemite Aerosol
751 Characterization study, *J. Geophys. Res., 110*, D14302, doi: 10.1029/2004JD005494.
752 McInnes, L., M. Bergin, J. Ogren, and S. Schwartz (1998), Apportionment of light scattering and
753 hygroscopic growth to aerosol composition, *Geophys. Res. Lett*., *25*, 4, 513-516.

754 Nenes, A., P. Y. Chuang, R. Flagan, and J. H. Seinfeld (2001), A theoretical analysis of cloud
755 condensation nucleus (CCN) instruments, *J. Geophys. Res.*, *106*(D4), 3449-3474.
756 Petters, M. D., and S. M. Kreidenweis (2006), A single parameter representation of hygroscopic
757 growth and cloud condensation nuclei activity, *Atmos. Chem. Phys. Discuss*., 6, 8435-8456.
758 Petzold, A., and M. Schönlinner (2004), Multi-angle absorption photometry - a new method for
759 the measurement of aerosol light absorption and atmospheric black carbon, *J. Aerosol Sci.*, *35*,
760 4, 421-441.
761 Pruppacher, H. R., and J. D. Klett (1997), *Microphysics of Clouds and Precipitation*, Kluwer
762 Academics, Norwell, Mass.
763 Rader, D. J. and P. H. McMurry (1986), Application of the tandem differential mobility analyser
764 for studies of droplet growth or evaporation, *J. Aerosol. Sci. 17*, 771-787.
765 Rissler, J., E. Swietlicki, J. Zhou, G. Roberts, M. O. Andreae, L. V. Gatti, and P. Artaxo (2004),
766 Physical properties of the sub-micrometer aerosol over the Amazon rain forest during the wet-
767 to-dry season transition – comparison of modeled and measured CCN concentrations, *Atmos.*
768 *Chem. Phys., 4*, 2119-2143.
769 Roberts, G., and A. Nenes (2005), A continuous-flow streamwise Thermal-Gradient CCN
770 chamber for atmospheric measurements, *Aeros. Sci. Technol., 39*, 3, 206-221.
771 Snider, J. R., and J. Brenguier (2000), Cloud condensation nuclei and cloud droplet
772 measurements during ACE-2, *Tellus, 32B*, 828-842.
773 Stokes, R. H., and R. A. Robinson (1966), Interactions in non-electrolyte solutions. I. Solute-
774 solvent equilibria, *J. Phys. Chem*., *70*, 2126-2130.
775 Topping, D. T., G. McFiggans, and H. Coe (2005), A curved multi-component aerosol
776 hygroscopicity model framework: 1 - Inorganics, *Atmos. Chem. Phys.*, 5, 1223-1242.

777 Twomey, S. (1977), *Atmospheric Aerosols*, Elsevier Scientific, 302 pp.

778 Weingartner, E., M. Gysel, and U. Baltensperger (2002), Hygroscopicity of aerosol particles at
779 low temperatures. 1. New low-temperature H-TDMA instrument: setup and first applications,
780 *Environ. Sci. Technol., 36*, 55-62.

781 Williams, P. I., M. W. Gallagher, T. W. Choularton, H. Coe, K. N. Bower, G. McFiggans (2000),
782 Aerosol development and interaction in an urban plume, *Aeros. Sci. Technol., 32,* 2, 120-126.

783 Zdanovskii, A. B. (1948), New methods of calculating solubilities of electrolytes in
784 multicomponent systems, *Zh. Fiz. Khim., 22*, 1475-1485.

Table 1a: Regression line parameters (intercept *a*, slope *b*) and correlation coefficients r^2 for calculated vs. measured CCN number concentrations using different input parameters in order to constrain the aerosol composition. All regressions are performed for the 400 data points for which a complete data set (S, $g(RH)$, $f(RH)$, and N_a) is available.

	S_1			S_2			S_3			S_4			S_5		
	a	*b*	r^2	*a*	*b*	r^2	*a*	*b*	r^2	*a*	*b*	r^2	*a*	*b*	r^2
$f(RH)_{blue}$	36	2.4	0.53	230	0.97	0.50	80	1.06	0.83	19	1.04	0.88	7	1.05	0.91
$f(RH)_{green}$	38	2.4	0.53	234	0.94	0.49	100	1.03	0.80	37	1.02	0.83	20	1.04	0.90
$f(RH)_{red}$	38	2.4	0.53	237	0.93	0.48	110	1.01	0.79	48	1.01	0.86	29	1.03	0.89
$g(RH)_3 \geq 137$ nm	46	2.7	0.53	215	1.16	0.57	66	1.22	0.91	38	1.12	0.90	18	1.13	0.94
$g(RH)_{all}$, 40-360 nm	52	3.3	0.55	263	1.26	0.57	106	1.27	0.91	80	1.14	0.90	52	1.14	0.93
Constant ε	68	2.3	0.42	262	0.95	0.51	96	1.10	0.88	64	1.05	0.86	60	1.06	0.88
nominal S values	106	1.8	0.38	305	1.08	0.47	112	1.13	0.84	62	1.07	0.90	42	1.08	0.91

Table 1b: Regression line parameters (intercept *a*, slope *b*) and correlation coefficients (r^2) for calculated CCN numbers using $f(RH)_{green}$ (Figure 3a) and $g(RH)_3$ as composition constraint (Figure 7)

	S_1			S_2			S_3			S_4			S_5		
	a	*b*	r^2	*a*	*b*	r^2	*a*	*b*	r^2	*a*	*b*	r^2	*a*	*b*	r^2
CCN number using $g(RH)_3$ *vs.* $f(RH)_{green}$	49	1.15	0.90	88	1.12	0.93	97	0.99	0.96	109	0.96	0.96	58	0.98	0.98

Table 2: Composition ($(NH_4)_2SO_4$/organic/EBC) and aerosol distribution details for individual periods (average)

#	Mass fractions			$\varepsilon_{predicted}$ based on $f(RH)_{green}$	Density [g cm^{-3}]	Mass loading [μg m^{-3}]	Particle number concentration [cm^{-3}]	Characteristics
	Inorganic $(NH_4)_2SO_4$	Organic	Equivalent black carbon (EBC)					
1	0.229	0.705	0.066	0.83	1.31	8.0	3961	
2	0.397	0.571	0.032	0.66	1.33	2.9	771	Clean, bimodal
3	0.660	0.328	0.012	0.32	1.49	17.7	4177	
4	0.693	0.279	0.028	0.38	1.38	4.8	1621	Fairly clean
5	0.17	0.805	0.025	0.79	1.18	9.4	10941	

Table 3: Relative importance of several parameters regarding CCN predictions for the data set at Chebogue Point during the ICARTT study (internally mixed aerosol population with homogeneous composition for size range)

Parameter	**Relative importance**
Size distribution	High
Supersaturation	High
Composition	Low
Size-resolved composition	Low
Insoluble fraction (number of soluble moles) as function of particle size	Moderate
(Organic) solute properties	Low

Figure captions

Figure 1: Schematic representation of model procedure. (The application of *g(RH)* as a composition constraint was performed in the same way.)

Figure 2: Measured growth factors for six particle sizes (40-360 nm) as a function of time. $g(RH)_3$ = average *g(RH)* for the three largest particle sizes, $g(RH)_{all}$ = average *g(RH)* for all sizes

Figure 3: Calculated vs. measured CCN number concentrations at five different supersaturations (S_1 ~ 0.07%, S_2 ~ 0.17%, S_3 ~ 0.27%, S_4 ~ 0.4%, S_5 ~ 0.5%); based on composition ($(NH_4)_2SO_4 + \varepsilon$) in order to match *f(RH)* at RH = 85%. a) λ = 700 nm ('red'); b) λ = 550 nm ('green'); c) λ = 450 nm ('blue'); - - - - regression line

Figure 4: Average size distribution of 400 data points (—— **;** left axis), and average scattering size distribution (right axis) at λ = 450 nm (——**);**λ = 550 nm (——**);**λ = 700 nm (——**);** g_1 and g_5 show the boundary sizes at which *g(RH)* has been measured, D_{crit1} and D_{crit5} are the average critical diameters for S_1 and S_5, respectively (ε = 0.63). Solid lines and dashed lines are for the dry and humidified distributions, respectively.

Figure 5: Predicted insoluble fraction, ε, based on *f(RH)* at three wavelengths, and on $g(RH)_3$. Predicted ε for *f(RH)* are color coded by wavelength. Black symbols: predicted ε for $g(RH)_3$;regression lines use the same color-coding; grey line: average ε based on $g(RH)_{all}$.

Figure 6: Calculated vs. measured CCN number concentrations at five different supersaturations (S_1 ~ 0.07%, S_2 ~ 0.17%, S_3 ~ 0.27%, S_4 ~ 0.4%, S_5 ~ 0.5%); based on composition ($(NH_4)_2SO_4 + \varepsilon$) in order to match $g(RH)_3$ at RH = 90%; - - - - regression line; ····· regression line based on composition in order to match $g(RH)_{all}$.

Figure 7: Calculated CCN number concentration based on composition ($(NH_4)_2SO_4 + \varepsilon$) in order

to match $g(RH)_3$ at RH = 90% vs. CCN number in order to match $f(RH)$ at RH = 85% (λ = 550 nm ('green')); - - - - regression line; ····· regression line based on composition in order to match $g(RH)_{all}$

Figure 8: Calculated vs. measured CCN number concentrations at five different supersaturations (S_1 ~ 0.07%, S_2 ~ 0.17%, S_3 ~ 0.27%, S_4 ~ 0.4%, S_5 ~ 0.5%); assuming a fixed composition of 37% $(NH_4)_2SO_4$/ 63% insoluble; - - - - regression line

Figure 9: Comparison of insoluble fraction calculated based on $f(RH)_{green}$ and measured mass fractions of EBC+organics (numbers = periods; Table 2); error bars represent the standard deviation of all ε for the individual data points in the respective period.

Figure 10: Calculated vs. measured CCN number concentrations at five different supersaturations (S_1 ~ 0.07%, S_2 ~ 0.17%, S_3 ~ 0.27%, S_4 ~ 0.4%, S_5 ~ 0.5%); based on $f(RH)_{green}$ and full composition information: open symbols: ($(NH_4)_2SO_4$ + ε); full symbols: composition as specified in Table 2, $\varepsilon' = 1$ (see text for details); - - - regression line.

Figure 11: Schematic of size distribution and critical diameters (vertical lines) and the assessment of relative uncertainty in predicted CCN number concentration; —— average size distribution, ····· cumulative size distribution.

Figure 12: Calculated vs. measured CCN numbers at five different supersaturations (nominal values of the CCN counter: S_1 = 0.09%, S_2 = 0.22%, S_3 = 0.32%, S_4 = 0.45%, S_5 = 0.55%) based on composition ($(NH_4)_2SO_4$ + ε) in order to match $f(RH)$ at RH = 85% (λ = 550 nm ('green')); - - - - regression line.

Figure 1

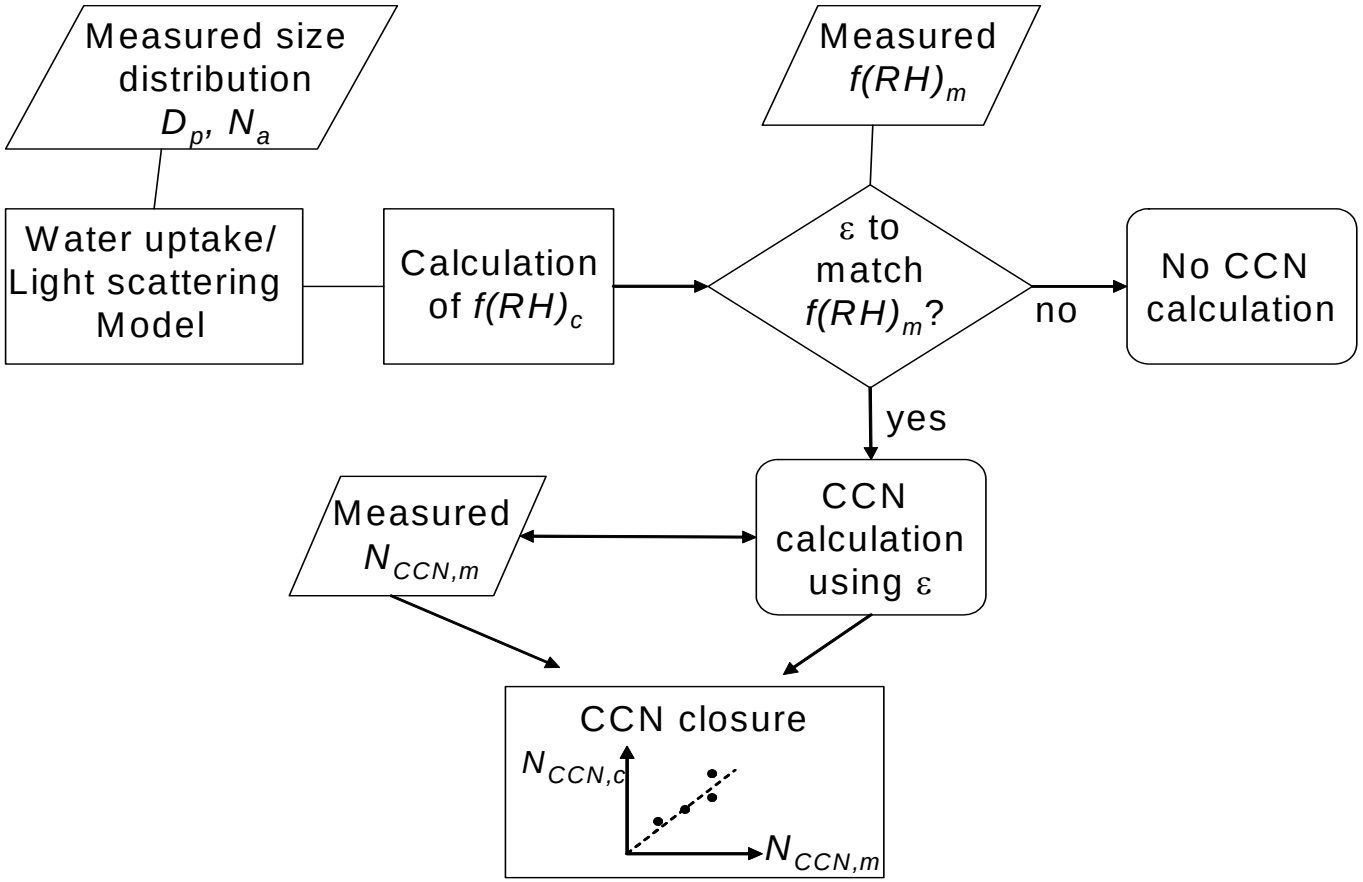
Measured size distribution D_p, N_a
Measured $f(RH)_m$
Water uptake/ Light scattering Model
Calculation of $f(RH)_c$
ε to match $f(RH)_m$?
no
No CCN calculation
yes
Measured $N_{CCN,m}$
CCN calculation using ε
CCN closure
$N_{CCN,c}$
$N_{CCN,m}$

Figure 2

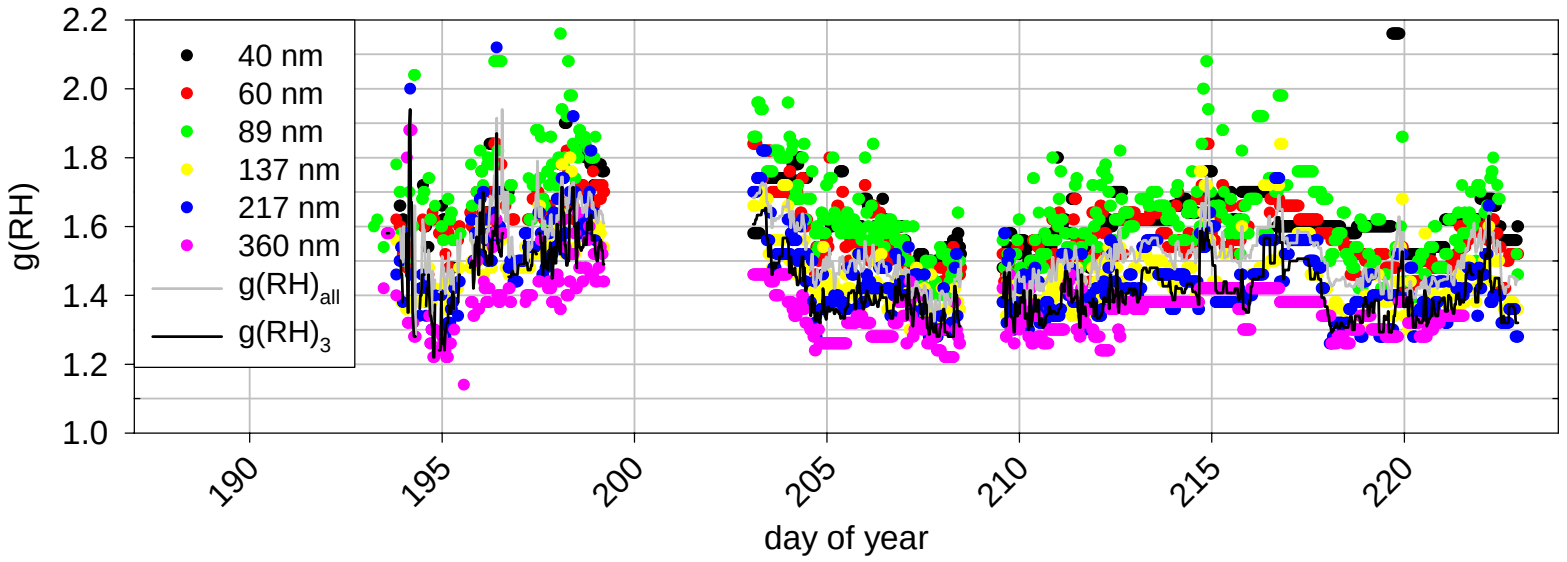
2.2
2.0
1.8
1.6
1.4
1.2
1.0
g(RH)
40 nm
60 nm
89 nm
137 nm
217 nm
360 nm
g(RH)all
g(RH)3
190
195
200
205
210
215
220
day of year

Figure 3

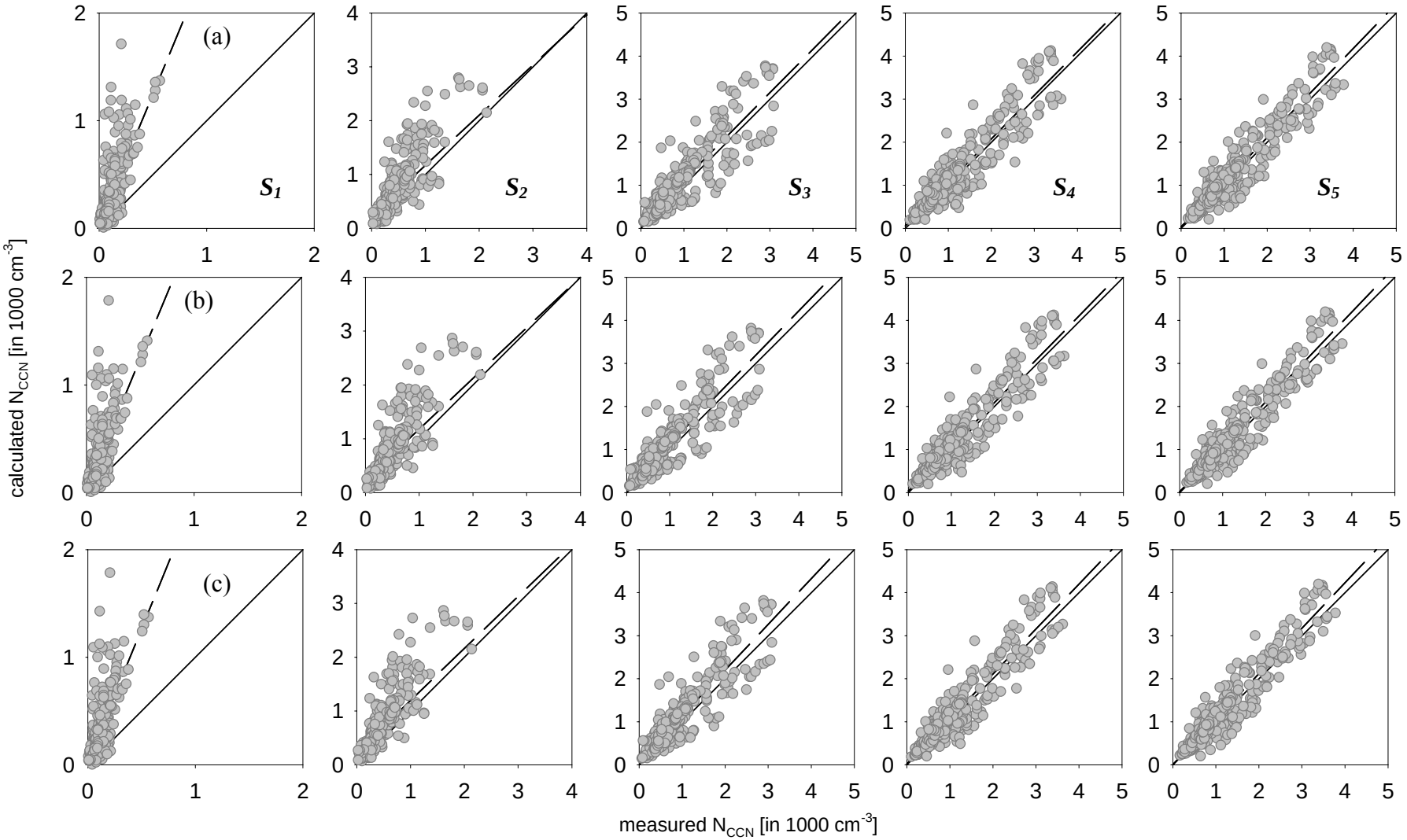
(a)
(b)
(c)
S_1
S_2
S_3
S_4
S_5
calculated N_{CCN} [in 1000 cm^{-3}]
measured N_{CCN} [in 1000 cm^{-3}]

Figure 4

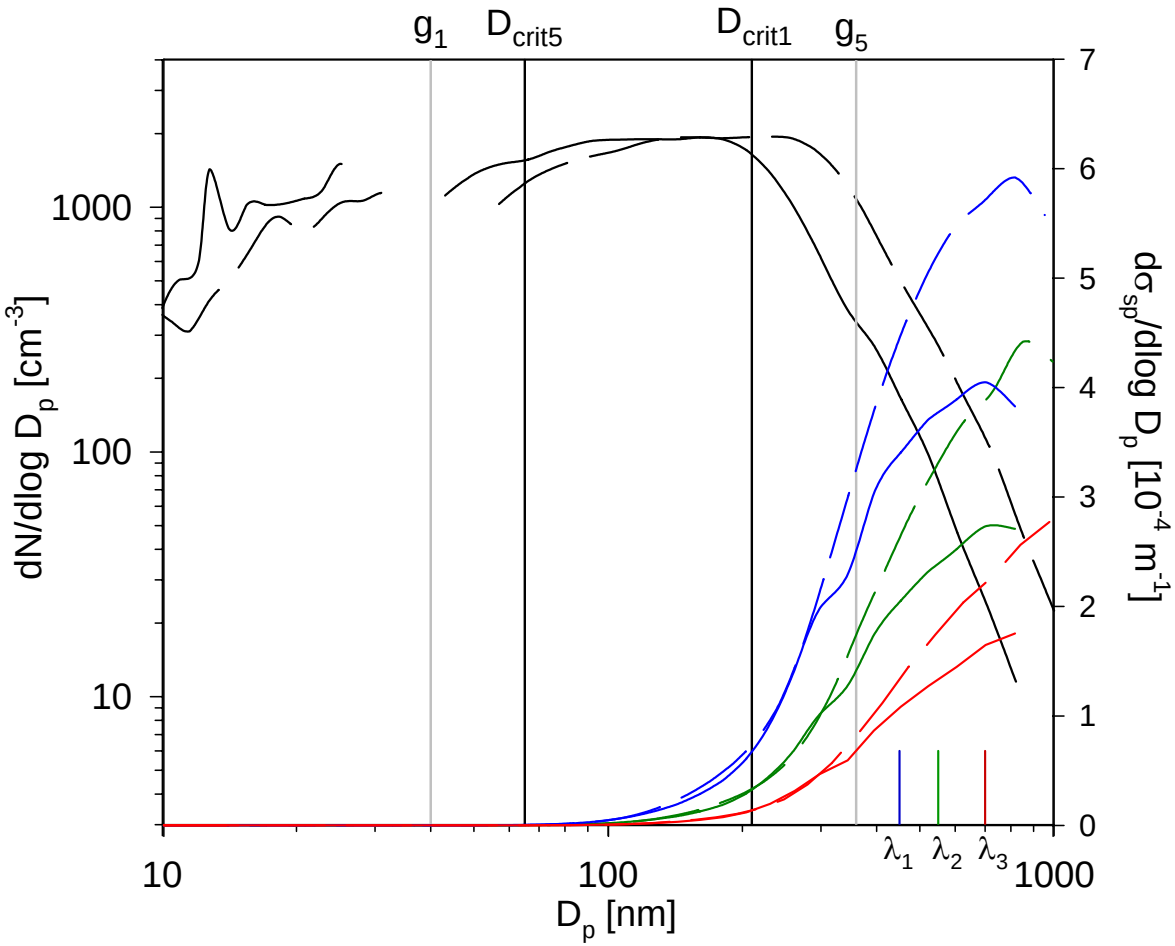
g1
Dcrit5
Dcrit1
g5
1000
100
10
dN/dlog Dp [cm-3]
7
6
5
4
3
2
1
0
dσsp/dlog Dp [10-4 m-1]
λ1
λ2
λ3
10
100
1000
Dp [nm]

Figure 5

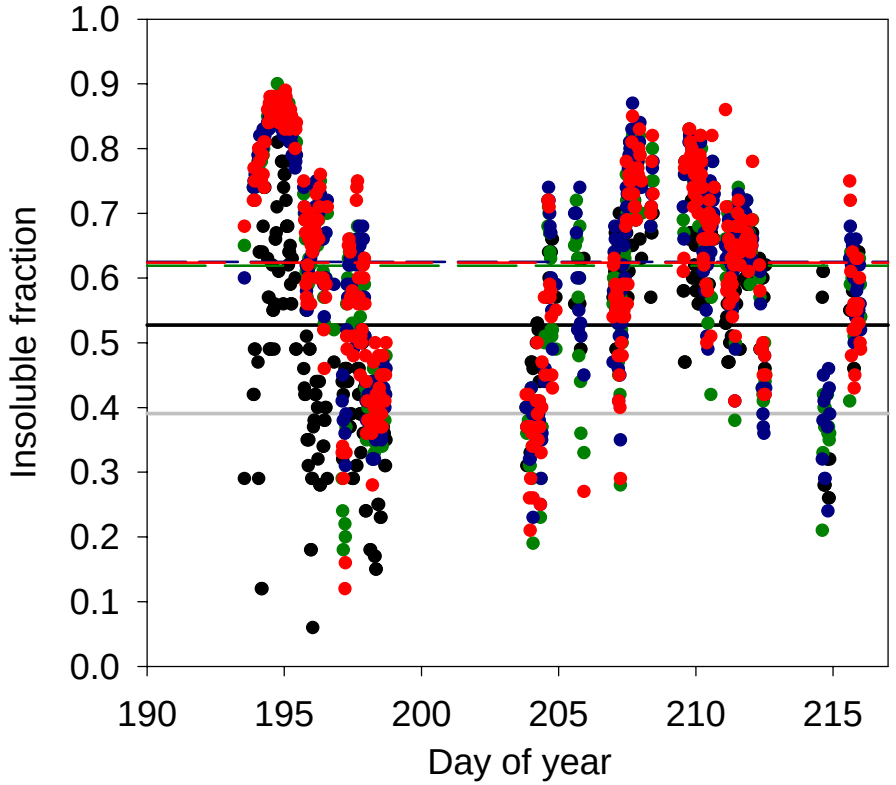
1.0
0.9
0.8
0.7
0.6
0.5
0.4
0.3
0.2
0.1
0.0
Insoluble fraction
190
195
200
205
210
215
Day of year

Figure 6

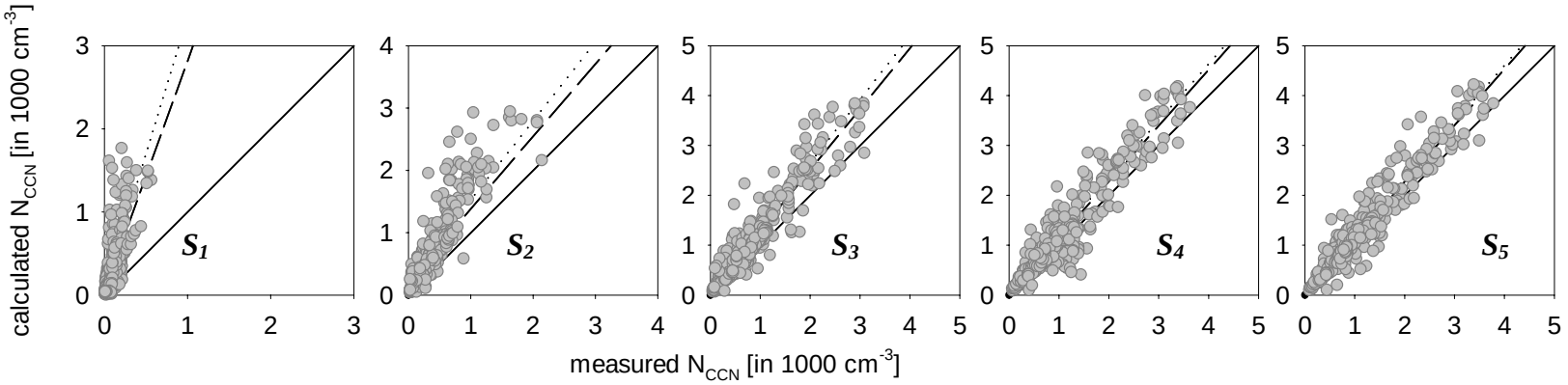
calculated N_{CCN} [in 1000 cm^{-3}]
measured N_{CCN} [in 1000 cm^{-3}]
S_1
S_2
S_3
S_4
S_5

Figure 7

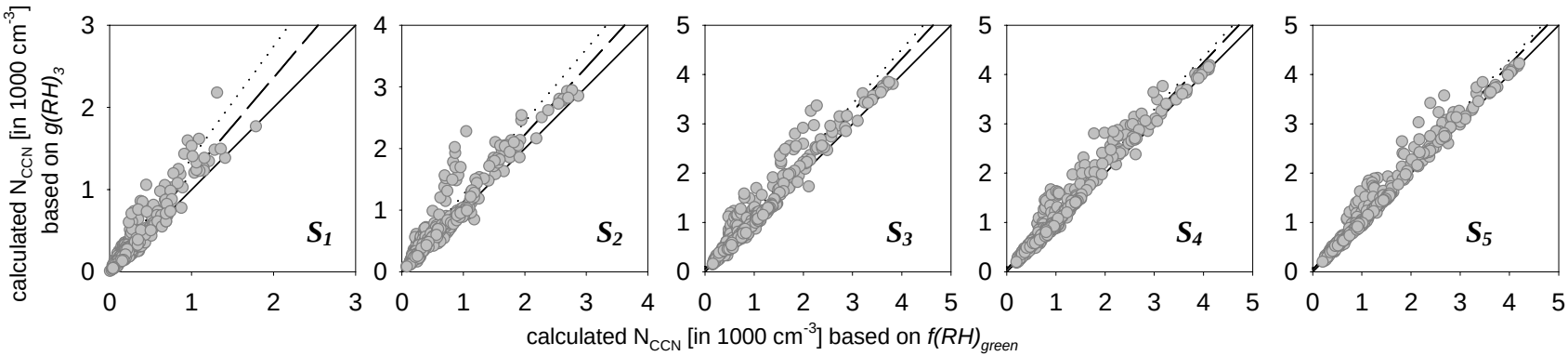
calculated N_{CCN} [in 1000 cm^{-3}] based on $g(RH)_3$
S_1
S_2
S_3
S_4
S_5
calculated N_{CCN} [in 1000 cm^{-3}] based on $f(RH)_{green}$

Figure 8

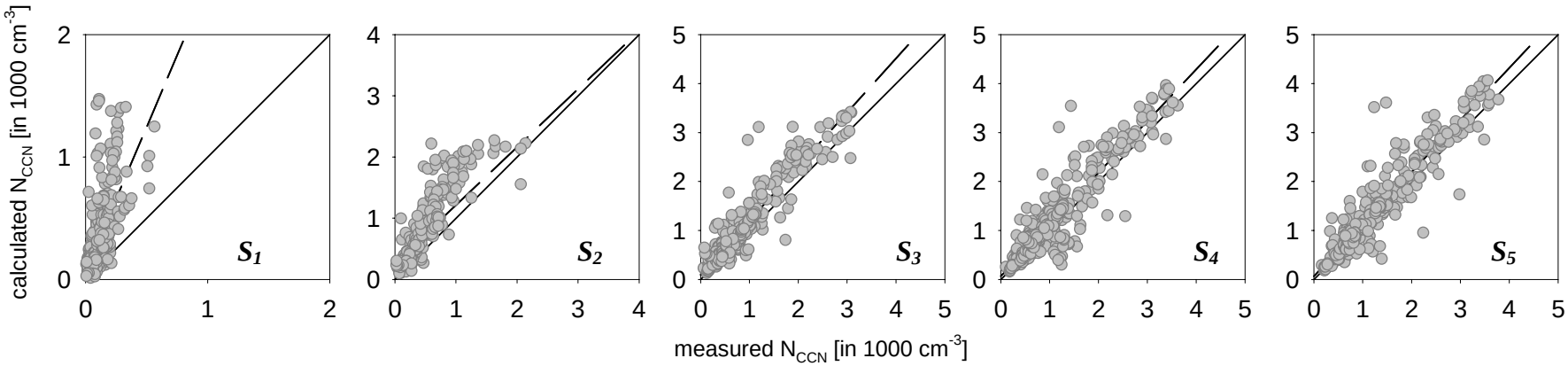
calculated N_{CCN} [in 1000 cm^{-3}]
measured N_{CCN} [in 1000 cm^{-3}]
S_1
S_2
S_3
S_4
S_5

Figure 9

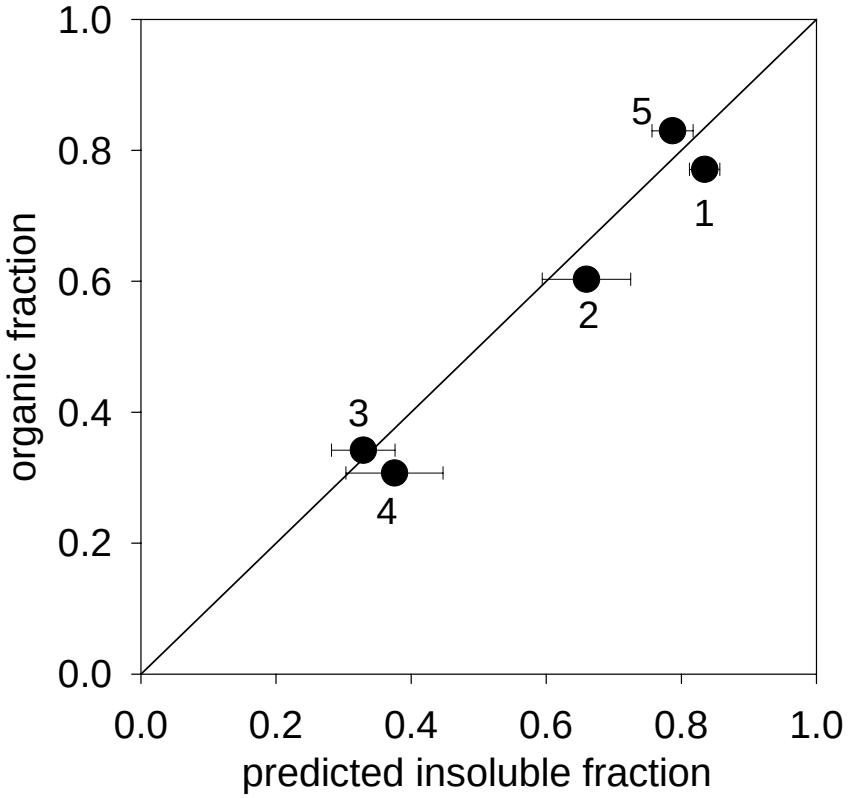
1.0
0.8
0.6
0.4
0.2
0.0
organic fraction
0.0
0.2
0.4
0.6
0.8
1.0
predicted insoluble fraction
1
2
3
4
5

Figure 10

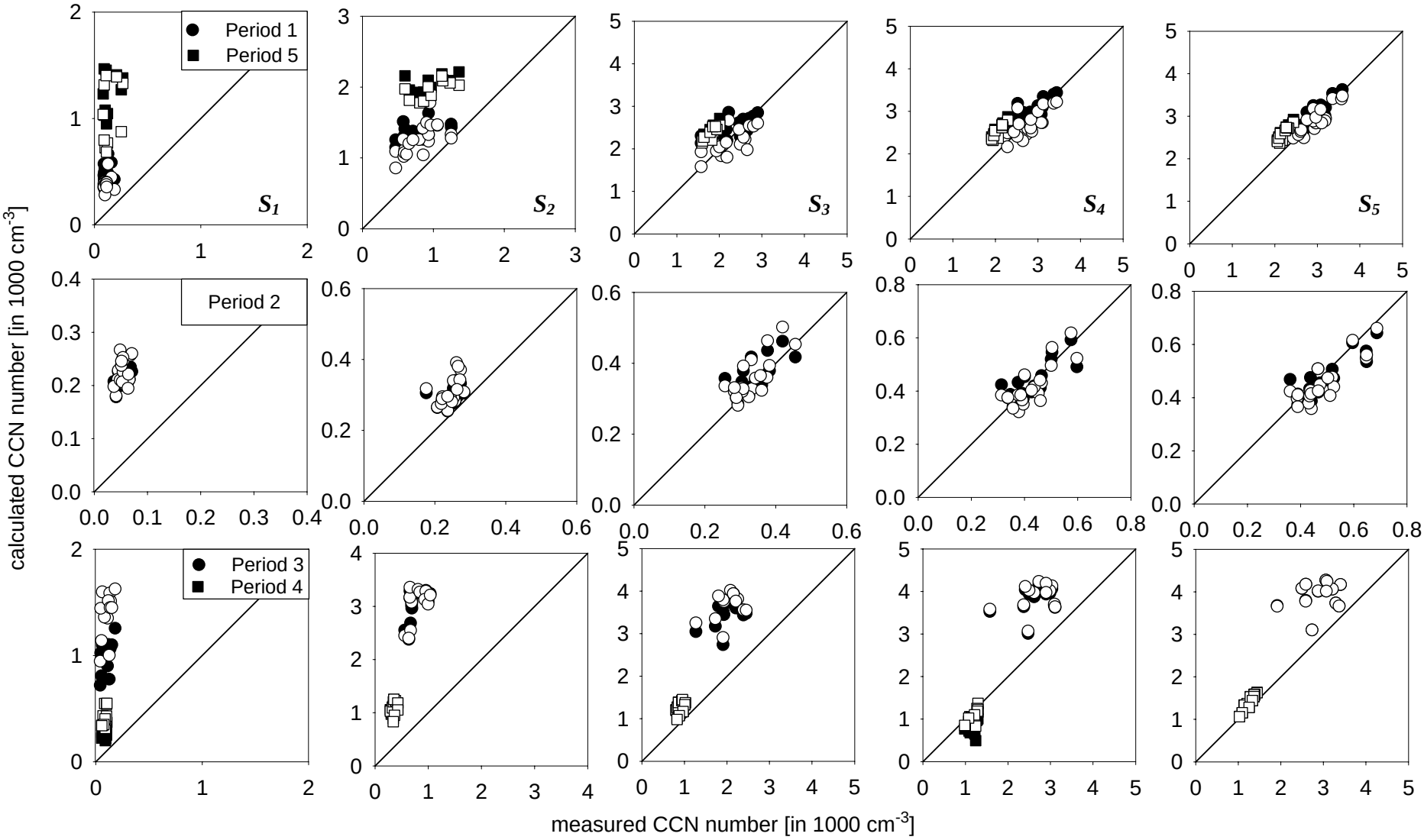
Period 1
Period 5
Period 2
Period 3
Period 4
S1
S2
S3
S4
S5
calculated CCN number [in 1000 cm-3]
measured CCN number [in 1000 cm-3]

Figure 11

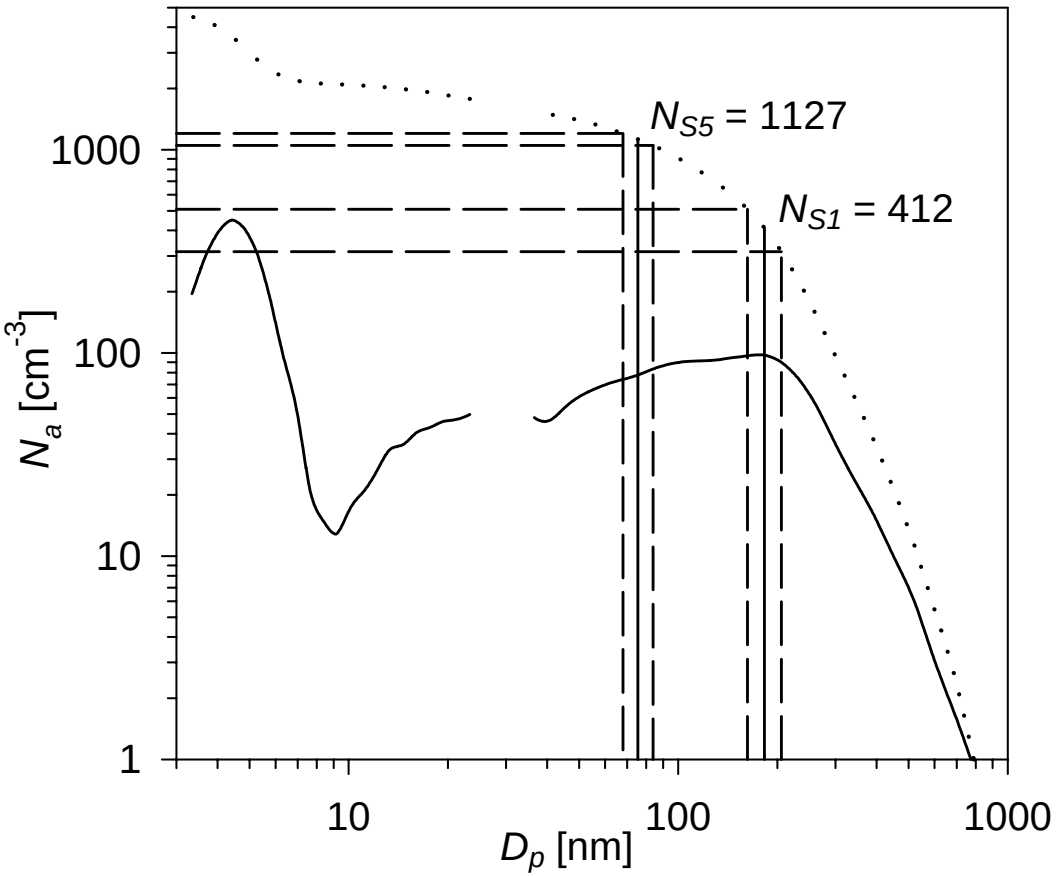

Figure 12

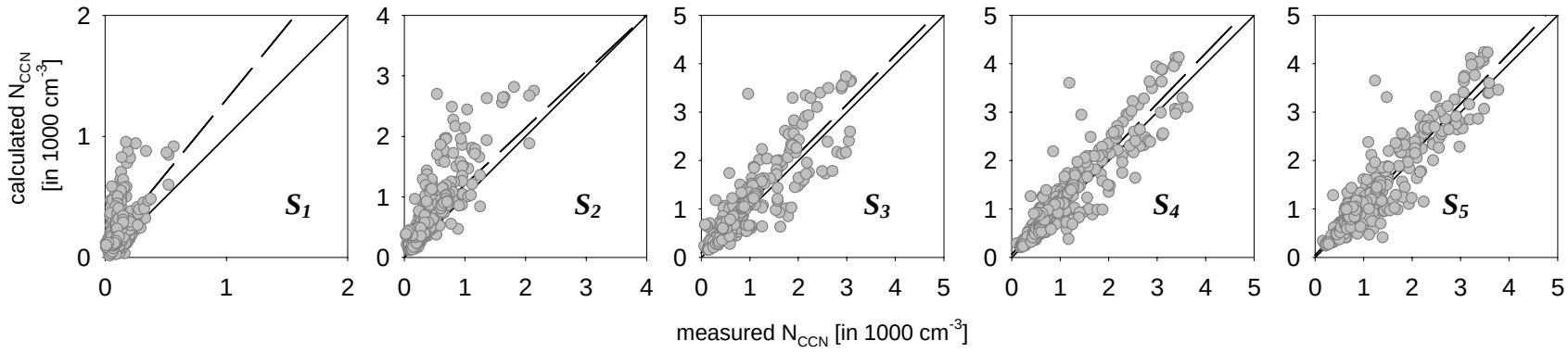
calculated N_{CCN} [in 1000 cm^{-3}]
measured N_{CCN} [in 1000 cm^{-3}]
S_1
S_2
S_3
S_4
S_5